SEIZURE DETECTION USING TEAGER-KAISER ENERGY AND A CHANNEL SIGNAL QUALITY ASSESSMENT ALGORITHM

by

Samuel Clary, B.S. Biomedical Engineering, B.S. Kinesiology

A Thesis Presented in Partial Fulfillment

of the Requirements for the Degree

Master of Science

COLLEGE OF ENGINEERING AND SCIENCE

LOUISIANA TECH UNIVERSITY

May 2019

LOUISIANA TECH UNIVERSITY

GRADUATE SCHOOL

April 5, 2019
Date of thesis defense

We hereby recommend that the thesis prepared by

Samuel Bennett Clary

entitled **Seizure Detection Using Teager-Kaiser Energy and a Channel Signal Quality Assessment Algorithm**

be accepted in partial fulfillment of the requirements for the degree of

Master of Science in Engineering, Biomedical Engineering Concentration

Dr. Levi Good, Supervisor of Thesis Research

Dr. Steven A. Jones,
Head of Biomedical Engineering

Members of the Thesis Committee:
Dr. Leonidas Iasemidis
Dr. Steven A. Jones

Approved:

Hisham Hegab
Dean of Engineering & Science

Approved:

Ramu Ramachandran
Dean of the Graduate School

GS Form 13
(01/19)

ABSTRACT

This study investigated the possibility of reducing the time required for accurate epileptic seizure detection through a retroactive analysis. Epilepsy is a neurological disorder affecting over 50 million individuals globally and is defined as a disorder which results in two seizures unprovoked by fever or medication. Diagnosis of epilepsy typically involves a monitored stay at an Epilepsy Monitoring Unit (EMU). The monitoring and diagnosis process ranges on average from $35,000 to $40,000 for a single stay, and the patient results from EMU are not instantly available to the patient. The collected electroencephalogram (EEG) must be analyzed by a trained EMU technician before the physician analyzes the data.

The retroactive seizure detection algorithm utilizes Teager-Kaiser energy (TE). TE increases as either a signal's frequency or amplitude increases and is only dependent on three consecutive samples from the time-domain. The detection algorithm was trained and tested on 37,718 hours of data from 70 male Sprague Dawley rats with a total of 843 recorded seizures. The algorithm resulted in an average sensitivity of 98.1% and an average false positive rate (FPR) of 0.2660 per hour. Current algorithms involve a training stage and perform with a sensitivity between 80% and 98.8% and a FPR between 0.054 and 1 per hour. The study supports TE as a useful measure for seizure detection, and although this algorithm focuses on retroactive seizure detection, the quick response time of TE makes it well suited for real-time seizure detection.

APPROVAL FOR SCHOLARLY DISSEMINATION

The author grants to the Prescott Memorial Library of Louisiana Tech University the right to reproduce, by appropriate methods, upon request, any or all portions of this Thesis. It is understood that "proper request" consists of the agreement, on the part of the requesting party, that said reproduction is for his personal use and that subsequent reproduction will not occur without written approval of the author of this Thesis. Further, any portions of the Thesis used in books, papers, and other works must be appropriately referenced to this Thesis.

Finally, the author of this Thesis reserves the right to publish freely, in the literature, at any time, any or all portions of this Thesis.

Author _____

Date _____

TABLE OF CONTENTS

LIST OF TABLES

LIST OF FIGURES

ACKNOWLEDGEMENTS

I am grateful to my Advisor and Committee Chair, Dr. Levi Good, for his support and direction and to my committee members, Dr. Leonidas Iasemidis and Dr. Steven Jones, for their guidance and advice.

Dr. Teresa Murray, Phillip Doughty, and Hayley Alexander deserve recognition for their critical involvement in the Louisiana Tech rodent study. Without these members, there would be no data to analyze.

Members of the Brain Dynamics Lab also have my gratitude for their advice with regard to the construction of the algorithms.

CHAPTER 1

INTRODUCTION

1.1 Epilepsy – History, Statistics, and Definition

Epilepsy is an ailment which the ancient Babylonians described nearly 3,000 years ago. The Greeks gave it its name meaning “received from the gods”, but Hippocrates rejected the idea that epilepsy was divine and realized that it was an ailment of the brain and the heart [1]. Even though this ailment has been known for centuries, it still remains prevalent and difficult to treat in the modern world. The ailment affects roughly 50 million individuals across the globe and 3 million Americans [2–4]. Modern medicine specifically defines epilepsy if at least two unprovoked seizures have occurred; therefore, seizures stemming from a fever or an improper diet are not classified as epileptic seizures [2], [4–6]. Epilepsy can result from sicknesses, improper cerebral development, or traumatic brain injuries. Cerebral damage from a stroke can also lead to the development of epilepsy; such forms of epilepsy are typically referred to as secondary or symptomatic epilepsy [2], [5], [7].

1.1.1 Epilepsy – Focal/Non-Focal

Epilepsy is classified into two main categories: focal (a.k.a. partial) or generalized epilepsy. Focal epilepsy refers to seizures that begin in one area of the brain, whereas generalized epilepsy to seizures that begin in both the left and right hemispheres of the brain and affects all brain regions at the same time. Sometimes a third category of

classification, multifocal epilepsy, is used. As the name implies, multifocal epilepsy begins in multiple discrete brain locations. All types of epilepsy involve groups of, rather than individual, neurons which, together with the "unpredictable" nature of seizure occurrences, magnifies the complexity of the ailment and presents many challenges for effective treatment [2], [4], [5].

1.1.2 Epilepsy – Sub-Classifications of Seizures

Many different types of seizures exist under the three main classifications of epilepsy, and each type of seizure tends to manifest in unique ways [8]. The number of existing seizure subtypes depends on which source is consulted [4], [5], [8]. The seizure subtypes as defined by Centers for Disease Control and Prevention will be discussed in the following sentences. Generalized epilepsy includes absence seizures (petit mal) and tonic-clonic seizures (grand mal). In absence seizures the patient may blink rapidly or stare blankly into the surroundings. Tonic-clonic seizures involve abnormal muscle activation and can result in loss of consciousness. Focal epilepsy presents three distinct seizure subtypes: a) simple focal seizures resulting mild muscle contractions or false sensations; b) complex focal seizures where consciousness is impaired and interpersonal interaction is inhibited; and c) secondary generalized seizures where seizures begin locally but eventually spread to other lateral or contralateral sides of the brain [8].

1.1.3 Epilepsy – Dangers

The impact of epilepsy on the patient's health depends on which groups of neurons in the brain are impaired. Since epilepsy affects the control center of the entire body, it can also result in abnormal psychological conditions such as peculiar sensations, emotions, and behaviors, yet physical effects, for example convulsions, muscle spasms,

and loss of consciousness, are also prevalent [2], [5], [7], [8]. The multifaceted nature of epilepsy results in a complex disorder that does not always trigger all these abnormal effects, but, typically, the consequences of an epileptic seizure pose a great risk to the individual in many different ways. Loss of consciousness or motor control are common sources of considerable injury. Finally, epilepsy does increase the risk of the life-threatening condition of status epilepticus (SE) or the condition of sudden unexpected death in epilepsy (SUDEP) [5], [9–11].

1.1.4 Epilepsy – SE & SUDEP

SE is defined as the condition with continuous seizures without a full conscious recovery between seizures. The high neuronal activity during SE places the individual at a much higher risk of excitotoxicity, a condition where neurons are destroyed as a result of an increased amount of glutamate [5]. Longer durations of SE are associated with more significant neuronal loss, and a history of SE is linked to an increased risk of SUDEP [9]. The cause of SUDEP is currently unknown; however, in addition to SE other risk factors for SUDEP, such as frequent tonic-clonic seizures and a lack of nocturnal supervision, have been identified. Timely administration of anti-epileptic drugs (AEDs) can avoid excitotoxicity and is thought to aid with SUDEP as well [5], [10], [11].

1.1.5 Epilepsy – Treatment Modalities

Brain scans can typically assist the diagnosis of epilepsy. Positron emission tomography (PET), magnetic resonance imaging (MRI), functional MRI (fMRI), and magnetoencephalography (MEG) scans are common clinical tools for diagnosis. Long-term EEG monitoring at EMU is usually the most revealing and useful tool for diagnosis and localization of the epileptogenic focus [6]. Once diagnosis has been accomplished, it

is highly advised to begin treatment right away because uncontrolled seizures could lead to further brain damage or loss of life. Currently, no cure exists for epilepsy, but pharmacological interventions have been successful in treating epileptic seizures. Some individuals can quit taking their medication after a few years, and their likelihood of going into remission remains low. Unfortunately, these cases usually resolve because of a spontaneous recovery from epilepsy rather than a cure brought about by medication [5–7]. Neuroregulatory devices implanted in the brain can be used to control epileptic seizures through a process known as neuromodulation, and pediatric epilepsy is even treated through a modified diet [6], [7]. Occasionally, a physician may recommend that the pathologically firing neuron be resected; however, resection is also a method of seizure control. It is not a cure for epilepsy [7].

1.1.6 Epilepsy – Diagnosis

Most diagnostic tests for epilepsy involve a monitored stay at a physician's office or a hospital. Typically, patients are monitored at specialized hospital units called EMUs. The stay at an EMU lasts longer than 24 hours on average, with some lasting up to six days. A single stay can be costly and result to a fee of $35,000-$40,000 [12]. Patients are typically tapered off the AEDs to manifest seizures while their multi-channel EEG and video are continuously recorded. Before the physician analyzes the recorded EEG and video, an EMU technician, trained to identify seizure activity, reviews the data and marks the times during which the patient exhibits physical signs of seizure activity. The current focus for reducing a patient's length of stay at the EMU is on the speed of seizure occurrence and recording [13].

1.2 Thesis Contribution

An accurate, automated method for seizure detection from the recorded EEG at EMUs could help alert caregivers of epileptic episodes, shorten the time of EEG analysis and diagnosis, and allow for seizure intervention through timely administration of AEDs or other timely neural or chemical interventions. Automated detection could also allow a physician to be notified faster of seizure activity and overall seizure trends. Automated seizure detection could also help with the treatment of SE and warn of upcoming SUDEP. Automated seizure detection could also reduce the amount of time a patient spends in an EMU. We developed a new seizure detection scheme with two consecutive stages that involve a) improvement of signal quality and b) detection of seizures from qualified EEG channels only.

1.2.1 Channel Signal Quality

A novel, multivariate multi-channel quality algorithm was implemented. The channel quality algorithm employs four different measures in both time and frequency domains from individual intracranial EEG (iEEG) channels. Channels are marked either with acceptable or non-acceptable signal quality.

1.2.2 Seizure Detection

Channels with acceptable signal quality were further analyzed for seizure events using a time series measure, the Teager-Kaiser energy (TE), estimated over running windows per channel. TE and three adaptive thresholds were used for seizure detection. Based on the performance of the seizure detection algorithm on training iEEG datasets, receiver operator characteristic (ROC) curves were created for each window duration to

determine to the optimal of the three thresholds as well as to, thereafter, select the best of the thresholds in terms of sensitivity and specificity of the achieved seizure detection.

CHAPTER 2

BACKGROUND

2.1 Channel Signal Quality – Current Techniques

Channel signal quality in EEG recordings has become a great concern over the years. The American Clinical Neurophysiology Society has even released guidelines for EEG recordings which directly address concerns of low quality data collection. These guidelines take into account electrode placement and materials [14]. Occasionally, avoiding a low quality signal is not possible. A damaged component which cannot be easily replaced can result in a low quality signal being present in an EEG recording. In this case, post-processing is required to identify channels with low signal quality. Some of the current channel signal quality algorithms are limited because they must be trained before accurate analysis of the subject's EEG can be performed [15]. The other methods of signal quality analysis detect low quality channels by comparing a single channel to all of the other channels in an EEG montage through correlation or through standard deviations from the mean of a statistical feature [16–18]. Assessing signal quality in this manner is reasonable, considering the number of electrodes used in human studies. Figure 2-1 displays the electrode placement for two human EEG montages.

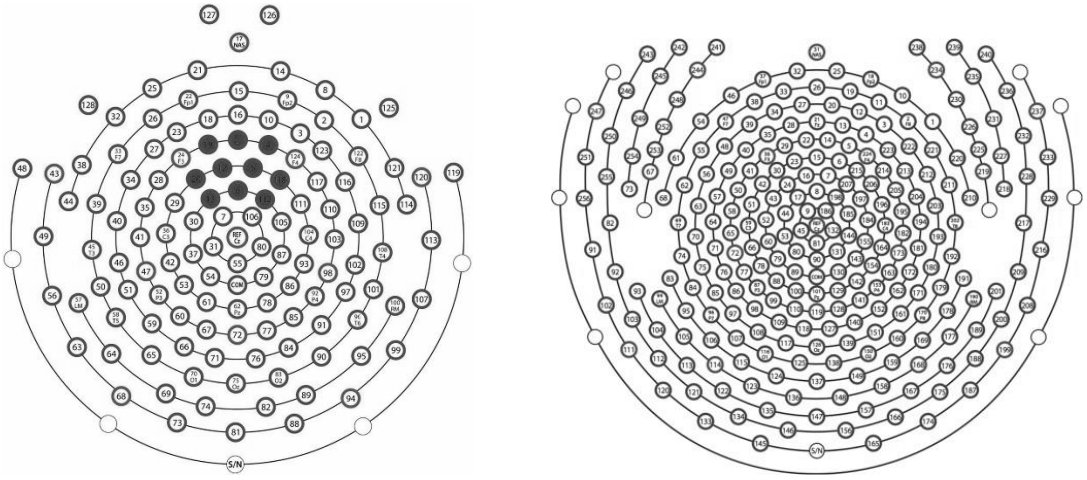

Figure 2-1: A human EEG electrode placements for a 128 channel montage (left) [19] and a 256 channel montage (right) [20].

In a montage with a high number of recording channels, comparing one channel to the others is an appropriate method for signal quality analysis; however, montages with a low number of recording channels, such as those in rodent studies, do not benefit from this approach using these methods. A few low quality channels can have a dramatic effect on the statistical comparison between one channel and the rest, which makes low signal quality channel classification difficult if not impossible.

2.2 Epilepsy – Seizure Detection Statistics

New methods for seizure detection are constantly being evaluated. The most important features of any such method are sensitivity, FPR, and, for real-time seizure detection, time delay. Sensitivity is defined as the ratio of correctly identified seizures to the total number of seizures; otherwise known as, the ratio of true positives (TP) to the sum of TP and false negatives (FN). FPR is defined as the ratio of the total number of incorrectly identified seizures, false positives (FP), to the total seizure free time, typically expressed as the number of FP per hour. FPR is used in place of 1-specificity, where

specificity is the ratio of true negatives (TN) to the sum of TNs and FPs, because the high number of TN, since seizures are relatively rare events, compared to the lower number of FPs produces potentially misleading results for specificity. It is possible for an algorithm to produce high sensitivity values while also having an alarmingly high FPR. Time delays are the time elapsed from a seizure to the time it was detected by the algorithm, typically in the order of seconds.

The current sensitivity for seizure detection algorithms from intracranial electroencephalography (iEEG) recordings is between 80% and 98.8%. The algorithms with the higher sensitivity are trained on data from the same patient they monitor. These algorithms cannot be used on other patients without first being trained on data for this patient. The FPRs vary greatly from 0.054 to 1 every hour. The time delay these algorithms have for seizure detection range from 20 seconds to 5 minutes [21–24]. A reduction in the time delay of a seizure detection algorithm translates to an individual receiving attention sooner from their caretaker, a lower risk for injuries, and a reduced possibility for evolution to SE or SUDEP [5], [11].

2.3 Epilepsy – Stages of iEEG Seizure Data

Seizure events typically have four stages: preictal, ictal, interictal, and postictal. Preictal stage refers to the immediate period prior to a seizure onset. The onset of the preictal period is not well-defined in the literature, either clinically, electrophysically, or mathematically. The ictal stage consists of the period from the beginning to the end of a seizure. Ictal periods usually start with a high frequency and low amplitude EEG, evolve a steady increase in the amplitude of an EEG signal, and end with a nearly instantaneous decrease in amplitude. The interictal stage is the period between seizures, in particular,

from the end of the ictal period of the preceding seizure to the beginning of the preictal period of the next seizure. The postictal stage is, like the preictal stage, not very well defined. Typically, the postictal stage immediately follows the end of a seizure and lasts until the subject has recovered. The beginning of this period is characterized by EEG suppression where the amplitude of the EEG signal is not only lower than the ictal stage but may be also lower than the one in the preictal stage. These stages can be seen in Figure 2-2.

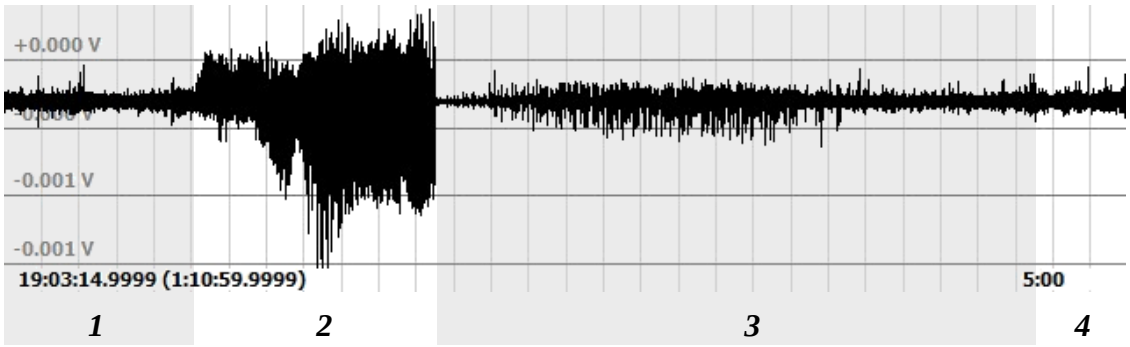

Figure 2-2: Seizure types (1) preictal, (2) ictal, (3) postictal, and (4) interictal from the iEEG data of one channel from one of our subjects.

In Figure 2-2, the portion of the data highlighted in section 1 is the preictal period; the portion highlighted in section 2 is the ictal period; the portion highlighted in section 3 is the postictal period; and the portion highlighted in section 4 is the beginning of an interictal period.

Because of these characteristic features of each stage of a seizure, an EEG technician can review several hours of EEG data in a matter of minutes. A seizure detection algorithm should be able to review several hours of EEG data in a matter of seconds if a reliable measure for amplitude and frequency is presented to it.

2.4 Epilepsy – Frequency Bands

To discuss the differences between EEG seizure trends and interictal EEG trends, the various commonly occurring EEG frequency bands must be discussed. Five main frequency bands exist. These bands are the delta, theta, alpha, beta, and gamma bands, and they range from less than 3 Hz, 4 to 7 Hz, 8 to 12 Hz, 13 to 30 Hz, and greater than 30 Hz, respectively. Frequencies around and between 5 and 15 Hz show the greatest separation between the power densities of ictal and non-ictal stages EEG data [25], [26].

CHAPTER 3

METHODS

3.1 Data

Louisiana Tech University's (LaTech) iEEG rodent studies involving male Sprague Dawley rats were employed for both channel signal quality analysis and seizure detection.

3.1.1 Recording of iEEG – Rodent Studies

Six cohorts of animals were recorded, with a seventh currently being recorded as of the creation of this report. Each cohort contained eight subjects. Some of the subjects of Cohort #6 did not survive and were replaced with other participants. Nine iEEG channels were used to record the cerebral activity of the subjects. The position of the recording sites in the brain of a rodent is depicted in Figure 3-1 below.

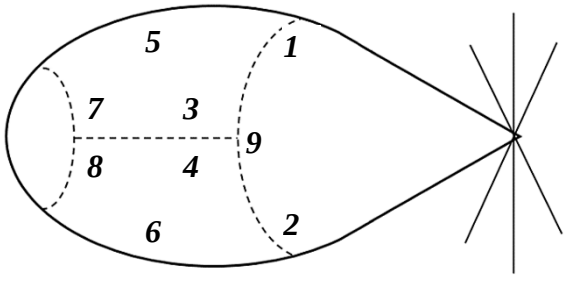

Figure 3-1: Schematic diagram of the iEEG electrode placements for the rodent studies.

The posterior portion of the skull in Figure 3-1 is towards the left, and the anterior portion of the skull is towards the right. The midsagittal suture is shown as the dashed horizontal line. Posterior to the midsagittal suture is the lambdoid suture, and the coronal suture is anterior of the midsagittal suture. As seen in Figure 3-1, eight electrodes were surgically inserted in each hemisphere within the pre-frontal cortex (1 & 2), the thalamus (3 & 4), the parietal cortex (5 & 6), and the hippocampus (7 & 8). Channel nine makes use of a bone screw which was implanted roughly 1 mm above the intersection of the midsagittal and coronal sutures; this channel is used as a reference channel. A tenth channel was used for ground without being attached to the subject.

The electrodes and the screw were held in place by a dental acrylic which bonded well with the skull while simultaneously providing a hardened cover to protect the cerebral cortex from trauma and infection. The electrodes extended up from the dental acrylic to a commutator which allowed the subjects to freely move about their housing by relieving the torsional forces on the wiring or the ends of the electrodes.

Once the electrodes had been implanted and secured, the subjects were injected with lithium to produce neuronal hyperexcitability and, within 24 hours, the subjects were injected with pilocarpine to inhibit neuronal pathways which utilize γ-aminobutyric acid (GABA). GABA is a prevalent neurotransmitter in the central nervous system that is responsible for neuronal inhibition. The GABA inhibits neuronal activity by decreasing the amount of neurotransmitters, such as chloride or calcium, that enter a neuron and preventing neurotransmitters from being released by the axon of the presynaptic neuron. If the release of GABA is hindered, the concentration of neurotransmitters will increase [27], [28]. Thus, the injection of pilocarpine caused the subjects to experience SE, which

typically leads to the development of epilepsy. Each cohort was recorded for an average of three months, and this led to over 800 seizures being collected, which were confirmed through visual inspection of the raw iEEG data by trained EEG technicians. The files containing the recorded iEEG data were initially collected with a recording duration of 24 hours for all data recorded before October 5th, 2017; these experiment groups include Cohort #1 and Cohort #2 as well as the beginning of Cohort #3. All recordings after this date were collected in 4 hour increments. The change in recording duration was implemented to reduce the impact of lower data quality which will be discussed in the following section.

3.1.2 TDT System Overview

The recorded data were collected using the System 3 with PZ5 NeuroDigitizer by Tucker Davis Technologies (TDT). The PZ5 allowed for 28 bits of resolution over an adjustable range that allows roughly 268 million unique data points to be recorded within a particular range. These unique values are always evenly distributed, but since the recorded values will rarely be exactly equal to one of the unique values, the recorded iEEG data is rounded to the nearest unique value. The high level of resolution caused these rounding errors to rarely be an issue. The TDT system sampled the iEEG data at roughly 2034.5 Hz, and the sampled data needed to then be converted into European Data Format (EDF) to be analyzed using MATLAB. This conversion process compresses the data into 16 bits of resolution, and when high amplitude artifacts were present, the compression to 16 bits along with the large dynamic range caused quantization errors in a few of the recordings.

Quantization errors were the first of two challenges regarding data quality. During compression, 15 bits were reserved for the resolution of the data while one bit was reserved for the sign. The compression allowed for 32,767 positive unique values to be stored and 32,768 negative unique values. The positive values had fewer placeholders because zero was included as one of the positive placeholders. These placeholders always represented uniformly distributed values from zero to the absolute value of the largest deviation from zero. The iEEG data were rounded to the nearest discrete value; therefore, if a high amplitude outlier was present in the data, the nearest discrete values became further spaced from each other [29]. The spacing produced iEEG signals with sharp transitions between plateaued sets of data points. In some cases, the quantization was negligible, but at other times the iEEG data were degraded to the point where analysis would produce meaningless results.

Quantization affects the entire recording period, and this effect was the major contributing factor to the decision of reducing the recording segment durations from 24 hours to every 4 hours. The decrease in recording times causes a smaller section of data to be lost if quantization occurs. Steps were also taken to identify the sources of these high amplitude artifacts. One contributing factor was the battery replacement in the system over 8 hours while the recording was active. Once the cause of this artifact was identified, the maintenance protocols were altered to pause the recordings during battery changes. Altering the protocol removed a considerable amount of these artifacts; however, the chance of a high amplitude artifact was not entirely removed.

Another challenge to data quality involved a channel or several channels which only recorded noise. There were several reasons for this error including dislocation of

iEEG electrodes through scratching or gnawing by the subjects and degradation of the physical components over time. The wiring was arranged in order to avoid being accidentally scratched by the subjects; however, since the wires had to connect to the subject's head, the wires could still be struck or caught and gnawed. The physical components which degraded tended to be the commutators. The constant movement of the subjects during the night would cause the metal contacts to wear away or have an intermittent connection in some cases. A few wires needed to be replaced throughout the course of the study.

Figure 3-2 shows examples of the power spectrum for what was classified as a good channel, and the power spectrum of a bad channel with noisy recording. These data quality issues necessitated the creation of a channel signal quality algorithm to evaluate the quality of the recording per channel. The algorithm operates on the following four metrics: a low to high frequency ratio, entropy, kurtosis, and a ratio of unique values to the total number of signal samples.

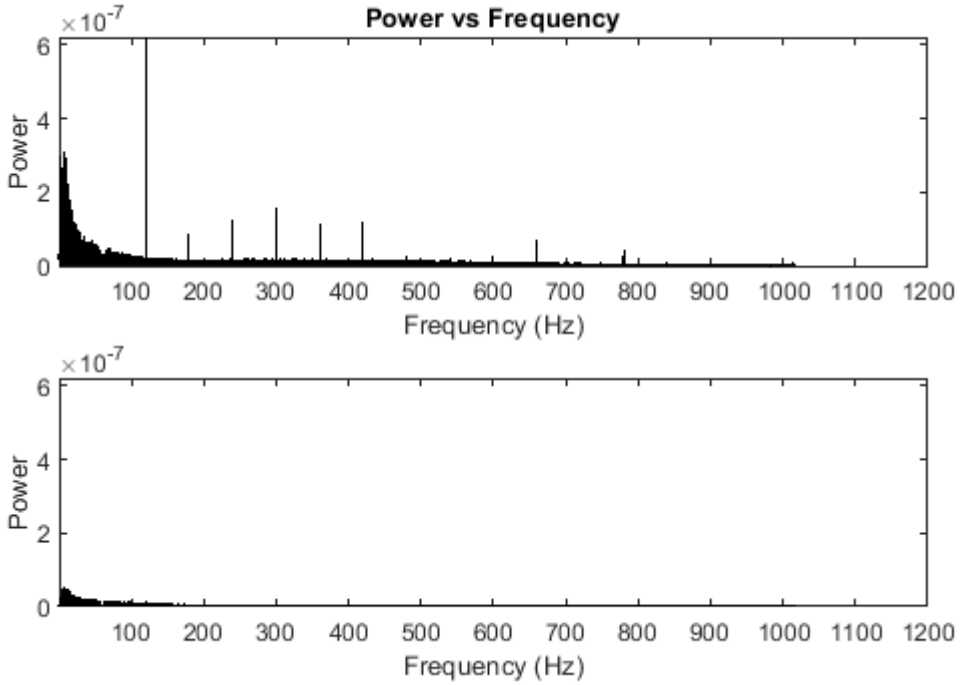

Figure 3-2: The PSD of an acceptable channel (top) and a noisy channel (bottom).

The PSD of the acceptable channel shown on top in Figure 3-2 has peaks at harmonics of 60 Hz line noise. The 60 Hz peak is not shown because it was filtered out by the TDT system. The amplitudes at frequencies less than 0.5 Hz are at such a high amplitude that displaying them would mask the power at other higher frequencies. Therefore, for clarity, the PSDs begin at 0.5 Hz and continues to the Nyquist frequency of ~1017.25 Hz.

3.1.3 Teager-Kaiser Energy

Time domain analysis increases the speed of a seizure detection algorithm since there is no need to transform the data into a different domain. A second advantage is the independence of the analysis from a particular frequency component of the signal especially when such a component is not the same across seizures and subjects. Both of

these aspects make a time domain analysis more robust when compared to a frequency domain analysis such as the use of Fourier transform.

Teager-Kaiser energy (TE) is a fast time domain measure of a signal's energy since it can be performed with only three sampled points as shown in Eq. 3-1. TE takes in consideration both the frequency and the amplitude of a signal. As the frequency or amplitude of a signal increases so does the value of TE. Eq. 3-1 shows how TE is calculated from a discrete signal, x, at a sample point, i.

$$TE = x_i^2 - x_{i-1}\, x_{i+1} \qquad \textbf{Eq. 3-1}$$

When calculating TE from a discrete signal with n points, the first and last TE values, $i = 1$ and $i = n$ respectively, are omitted because the raw data values for x_0 and x_{n+1} do not exist. When applied to a cosine signal, $A\cos(\Omega_i + \phi)$, where variables A, Ω, and ϕ are the amplitude, the digital frequency ($\Omega = 2\pi f/F_s$, $f =$ analog frequency, $F_s =$ sampling frequency), and the phase respectively, TE is:

$$TE = A^2 \sin^2(\Omega) \qquad \textbf{Eq. 3-2}$$

As long as Ω is less than a fourth of the sampling frequency, TE is closely approximated, with a maximum of 11% error, as:

$$TE = A^2\Omega^2 \qquad \textbf{Eq. 3-3}$$

This equation is instructive for TE's relation to the amplitude and angular frequency of a signal [30], [31]. Since the iEEG data were sampled at roughly 2034.5 Hz and the highest frequencies analyzed were 15 Hz, the approximation that leads to Eq. 3-3 can be used. For the parameters used in this study, the approximation is appropriate for frequencies up to roughly 508.6 Hz.

3.2 Data Pre-Processing

Both the channel signal quality algorithm and the seizure detection algorithm preprocessed raw iEEG data from our rodents. Both algorithms used Butterworth bandpass filters with different cutoff frequencies and the filter orders. These filters were applied in both the forward and reverse directions to construct zero phase filters. Whereas the bidirectional filtering allows for zero phase distortion, the filter order becomes doubled due to the bi-directional nature of the filtering.

3.2.1 Channel Signal Quality

The channel signal quality algorithm analyzed frequencies only between 1 Hz and 220 Hz; therefore, a third order, Butterworth bandpass filter with cutoff frequencies at these respective values was applied to the data. (Because of the filtering method, this bandpass filter was effectively a sixth order filter.)

3.2.2 Seizure Detection

Since the greatest separation of power between ictal and non-ictal periods is typically manifested between 5 Hz and 15 Hz, a fourth order Butterworth bandpass filter was applied to the iEEG data, with cutoffs at these respective frequencies. (As with the previous filter, the employed technique results in an eighth order filter.)

3.2.3 Battery Artifact Removal

A separate data quality algorithm had to be created to compensate for the battery replacement artifact. Figure 3-3 shows an example of the effect of a battery replacement on the raw EEG data.

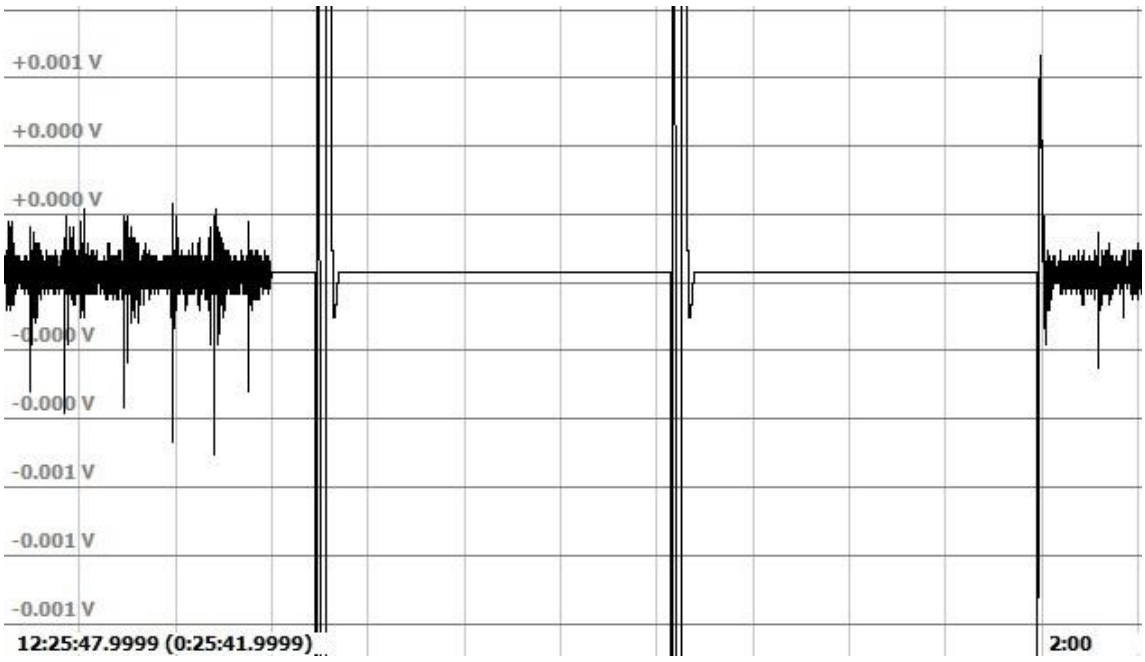

Figure 3-3: A 2 min recorded EEG with a battery replacement artifact.

The vertical axis in Figure 3-3 is divided into increments of 0.2 mV. Changing the battery produced a huge high amplitude artifact that resulted to flat-lined iEEG data. The high amplitude artifact was regularly outside of the amplifier's $\pm$0.5 V range, nearly three to four orders of magnitude larger than the iEEG signal. This event can also be caused by a loose or damaged physical connection in the electrodes themselves or the cables that connect the subject to the TDT system. Fortunately, this type of event was not difficult to detect and remove. An algorithm was designed to search for flat-lined data. The algorithm searched for consecutive points with identical values. The simple method of detection was effective since EEG data varies dramatically from sample point to sample point during high signal quality. All the detected points were removed from analysis and a buffer of six data points was removed from each side of the flat-lined data to fully remove the artifacts.

3.3 Channel Signal Quality

Each of the four metrics of signal quality was calculated over 15 minute non-overlapping running windows on every channel. A median value for each metric was subsequently determined over these running windows, and these median values were used in the optimization process. The frequency ratio and entropy metrics were used in combination to detect noisy data, and the kurtosis and unique ratio metrics were used to detect quantization errors.

3.3.1 Noisy Data – Frequency Ratio

Detection of a noisy recording was first tested by using the measure of a ratio of low to high frequencies. The range of low frequencies considered was 1 and 110 Hz, and the range of high frequencies was between 110 and 220 Hz. The discrete Fourier transform (Eq. 3-4) via fast Fourier transform as implemented in MATLAB's function, fft, was used to estimate the powers at these frequencies.

$$\hat{X}(k) = \sum_{n=-\frac{N}{2}}^{\frac{N}{2}} x(n\,T_s)\; e^{-j\left(\frac{2\pi}{N\,T_s}k\right)n\,T_s} = \sum_{n=-\frac{N}{2}}^{\frac{N}{2}} x(n)\; e^{-j\frac{2\pi k}{N}n} \qquad \textbf{Eq. 3-4}$$

In this equation, n is a particular time value with a window of length $N \cdot T_s$ of x, the iEEG signal. $\hat{X}$ is the power spectrum density (PSD) that corresponds to the power at the angular frequencies in radians per second, $k \cdot \frac{2n}{N \cdot T_s}$, where $T_s = \frac{1}{f_s}$ and f_s is the sampling frequency in Hz [32]. The power densities at the low frequencies were summed and divided by the sum of the powers at the high frequencies to estimate the metric of the frequency ratio.

In this metric, a value close to 0 is indicative of noise in the data because lower frequencies lack the high power that is characteristic of iEEG. Consequently, a high valued ratio would imply a channel containing high signal quality iEEG data.

3.3.2 Noisy Data – Entropy

A second test for noise in the data used time series entropy values. Entropy was calculated using Eq. 3-5.

$$S(X) = -\sum_{i=1}^{N} p(x_i)\ln\big(p(x_i)\big) \qquad \textbf{Eq. 3-5}$$

In this formula, x_i are the iEEG values in a data segment, X is a particular range of x_i values, $p(x_i)$ is the probability of appearance of value x_i in the data segment. The hypothesis was that noise produces high entropy values because then the spectrum is flatter, indicative of the signal being at a state more similar to white noise (maximum entropy).

3.3.3 Quantization Error – Kurtosis

The first test for detecting quantization errors was based on kurtosis measurements (Eq. 3-6).

$$k = \frac{E(x-\mu)^4}{\sigma^4} \qquad \textbf{Eq. 3-6}$$

Where x are iEEG values, μ is the mean of x, σ is the standard deviation of x, and $E(t)$ is the expected value of X. Quantization shifts x values towards the center of the generated histogram from the x data. The shifted values narrow the histogram while simultaneously increase its height. The edges of the histogram had fewer values (ie. less probability density) in their bins thus producing a kurtosis value higher than 3. Taking in

consideration that normal distribution has a kurtosis value of 3, a higher kurtosis value than 3 indicated possible quantization errors.

3.3.4 Quantization Error – Unique Ratio

The second test we used for quantization error detection was the ratio of unique values to the total number of sample points. Quantization has an effect similar to rounding, that is, a blocky signal is created with values most closely match, the signal's original values. Quantization therefore reduces the number of unique values in a given signal. After quantization, by counting the number of unique values via MATLAB's unique function (unique) and dividing by the total number of sample points in a given period, we formed a ratio that was inversely related to the potential presence of quantization errors.

3.3.5 Optimization – Training Data

Each of the above metrics was optimized from training data consisting of 704 iEEG channel segments with each segment having an average duration of 3.41 hours and a standard deviation of 1.15 hours. These segments were chosen from 88 randomly selected files from Cohort #1 to Cohort #5. All segments were visually inspected for clearly occurring quantized and noisy data. The segments were appropriately labeled as low quality channels. The number of segments with high signal quality totaled to 399 segments. The number of noisy and quantized segments were 137 and 168, respectively.

Then, a unique set of 100,000 thresholds was created for each of the four metrics to evaluate the previously accessed signal quality segments. These thresholds determined if a segment would be classified as having high signal quality rendering a value of 0 or low signal quality rendering a value of 1. If the entropy, frequency ratio, or unique ratio

metric values were above their respective thresholds or if the kurtosis value was below its assigned threshold, the segment was marked with 0. All other segments were marked with 1. This process produced a two-dimensional binary matrix with dimensions equal to the number of thresholds by the number of segments.

These matrices were then paired to address the two challenges of signal quality. In particular, the binary matrix for entropy was paired with the binary matrix for the frequency ratio, and the binary matrix for kurtosis was paired with the binary matrix for the unique values ratio. The matrices in a pair were combined by taking the sum of a threshold row from the first matrix with the sum of a threshold row from the second matrix. The process of combining the matrices was repeated until all threshold rows from one matrix in a pair had been summed with all of the threshold rows from the second matrix. The resulting combined matrix was three dimensional of size equal to the length of the thresholds from the first matrix by the length of the thresholds from the second matrix by the length of the segments for both matrices. The three dimensional matrices were formed through summation as opposed to multiplication to increase the likelihood of TPs. The drawback of this method was the likelihood of generating higher numbers of FPs.

The TP, FP, TN, and FN values were calculated for every combination of thresholds. Thus, we could estimate sensitivity and specificity values for every combination of thresholds. The sensitivity and specificity values enabled the construction of an ROC analysis. The upper left corner in an ROC plot represents 100% sensitivity and 100% specificity; therefore, a shorter distance from this point to any point on the

ROC curve represents a more ideal combination of thresholds. Eq. 3-7 was used to calculate this distance.

$$\text{Distance} = \sqrt{(\text{Sensitivity} - y_d)^2 + \left((1 - \text{Specificity}) - x_d\right)^2} \qquad \textbf{Eq. 3-7}$$

The distance to the upper left corner was calculated for every ROC value from every threshold combination. The desired Cartesian coordinates for the x-axis and y-axis were defined as $x_d = 0$ and $y_d = 1$ respectively. The shortest distance for each quality issue was estimated, as was the threshold combination associated with this distance.

3.3.6 Optimization – Testing Data

Once the algorithm had been optimized for the training data, it was applied to testing data composed of 1,216 randomly selected iEEG channel segments with a mean duration of 3.91 hours and a standard deviation of 2.76 hours. These segments were selected from 152 files from Cohort #1 to Cohort #5. It was taken care that these segments did not overlap with any of the previous 704 segments from the training data to avoid within sample bias. Of the testing segments, 591 had high signal quality, 257 were categorized as noisy, and 368 were categorized as quantized.

Similar to the training data, the testing data were first visually inspected for quantization and noise free quality. The segments with low signal quality were sorted into the respective quality category, and all other segments were labeled as good quality segments. Using the visual analysis results and the results from the algorithm, the TP, FP, TN, and FN values were calculated for the testing data. Channels with good quality segments were then subjected to the next processing stage for seizure detection.

3.4 Seizure Detection

The seizure detection algorithm first estimated TE from non-overlapping 30 second windows in channels of good quality as determined by the channel signal quality algorithm. The median TE value over all channels was then calculated at each time point. The median values were assembled into one signal to further analyze using three separate algorithms with their own dynamic threshold for seizure detection.

3.4.1 Optimization – Training Data

To train the seizure detection algorithm, four days of data were randomly selected from every subject in every cohort. The selected files rate contained 103 visually discerned seizures out of a total of 4,981.8 hours of data. Three adaptive thresholds were tested to detect significantly high TE values when seizure activity was present. Each threshold was estimated from a series of overlapping windows ranging from 90 to 1,500 seconds, corresponding to 3 to 50 median TE points.

The threshold value from each of the overlapping windows was calculated using equal parts past and future data. Real-time analysis does not allow thresholds to be constructed in this manner since the future values cannot be used, but retroactive analysis allows for the use of future points. A threshold created using past and future points reduces the number of false positives when non-seizure amplitude shifts occur as seen in Figure 3-4.

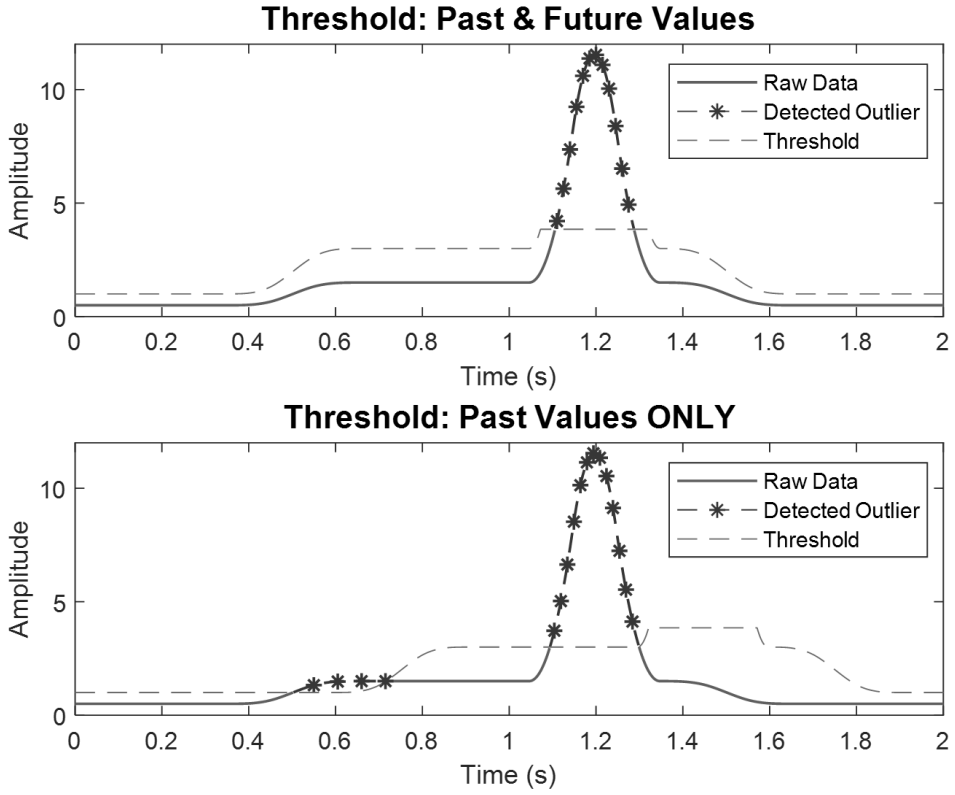

Figure 3-4: Effects of past and future values on threshold creation for event detection.

The threshold in Figure 3-4 is created by a moving average with a window size of 0.5 seconds and a scaling factor of 2. The only desired detection occurs at 1.2 sec, and all other detections are FPs. If past values are exclusively used to create an adaptive threshold, as in the lower graph of Figure 3-4, the threshold is delayed which results in the FP at 0.6 seconds as a consequence of the undesired amplitude shift. A threshold composed of equal parts of past and future points, the upper graph of Figure 3-4, lacks a delay and is resistant to undesired amplitude shifts. For these reasons, both past and future points were used in the creation of all three adaptive thresholds.

The first threshold involved the interquartile range (IQR) and was created by modifying a common outlier detection method, the 1.5 IQR Rule. In a normal

distribution, the probability of a value occurring outside of this acceptable range is 0.7%. Since a higher TE value is assumed to be a seizure, we used a single tailed approach, and this probability of not detecting a seizure was reduced to 0.35%. The equation for this threshold is:

$$\text{Theshold} = Q3 + IQR \cdot sf \qquad \textbf{Eq. 3-8}$$

Where $Q3$ denotes the third quartile of the distribution of the median TE values. The IQR is defined as the difference between $Q3$ and the first quartile ($Q1$). The IQR and $Q3$ were determined for each window, and then, the IQR scaling factor (sf), typically 1.5, was varied between 1 and 158.5 or 0 and 2.2 on the logarithmic scale to reach the corners of the ROC plots.

The second threshold we tested was created using a scaled median value. Scaling just the median TE themselves was attempted after visual inspection indicated that TE values around seizure events tended to be much higher than at other time points. The median TEs were scaled by a factor that varied between 1 and 158.5 or 0 and 2.2 on the logarithmic scale.

The third threshold we tested was based on a median and scaled standard deviation. This threshold was inspired by the $\bar{X}$ and $\bar{S}$-Charts used in Six-Sigma applications where the upper control limit is defined as the mean plus the scaled standard deviation. Since the median is less sensitive than the mean to noises, the median of TE was implemented in place of the mean in the formulation of this threshold. A median value as well as the standard deviation were calculated for every window from the TE time series. Once these values were determined, the standard deviations were scaled by a factor which varied between 1 and 158.5 or 0 and 2.2 on a logarithmic scale, and the

scaled standard deviations were then added to the medians. These added values then became the third threshold we tested for seizure detection.

Each of the three thresholds were used to acquire sensitivity and FPR results for the ranges of window length and scaling factor. These sensitivity results and FPRs were then used to construct the respective ROC sensitivity verses FPR curves of seizure detection. These curves were then analyzed to find the optimal window length and scaling factor, that is, the ones that rendered close to 100% sensitivity and zero FPR in seizure detection. We used the same approach to optimization as in the signal quality methodology. The above scheme was applied to raw iEEG data from: a) good channels only where both quantized and noisy ones were excluded, b) good channels where only noisy ones were excluded, and c) all available channels, high and low quality, were included.

The sensitivity and FPRs were calculated for each subject first. Once the sensitivity and FPR matrices were calculated, a mean was taken across all subjects. The next step involved testing all combinations of sensitivity and FPRs to determine which point on the ROC plots had the shortest distance to the upper left corner. When this point was determined, the window size and the threshold offset associated with the point were determined and stored.

3.4.2 Optimization – Testing Data

The testing data consisted of 32,736.8 hours of continuous multi-channel iEEG data from 70 rats containing a total of 740 seizures that was compiled from the remainder of the cohort data that were not included in the training data set for seizure detection. The optional window size and scaling factor determined from the training data were used on

the testing data. The sensitivity and FPR that corresponded to these optional parameters were then calculated for three cases: a) no quantized and noisy channels, b) no noisy channels, and c) all available channels. The three cases were run on the testing data to test their consistency with the training results. The flowchart with all different stages of the training of the seizure detection algorithm is shown in Figure 3-5.

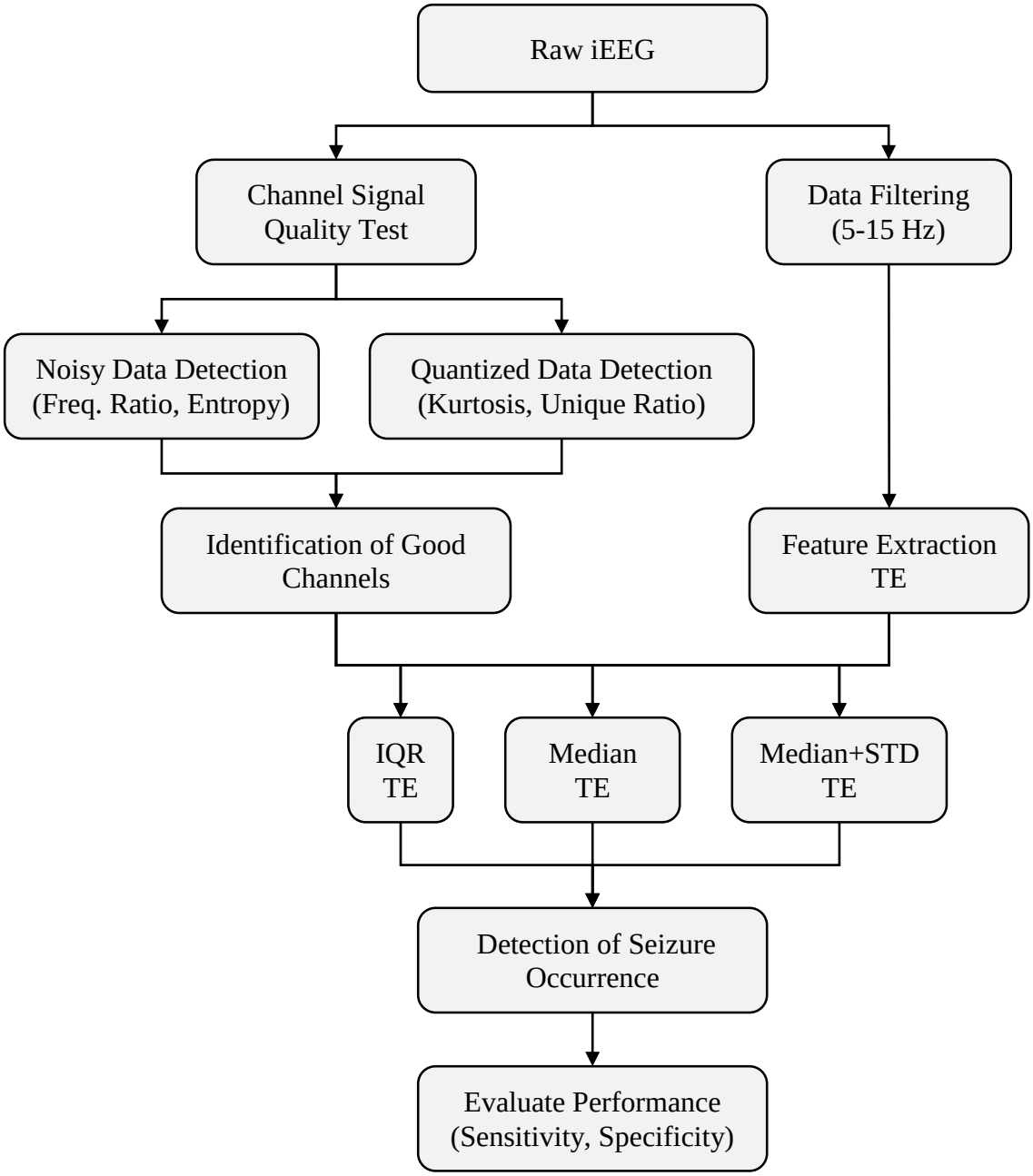

Figure 3-5: Flowchart with the stages of training of the seizure detection scheme.

The final flowchart of the seizure detection algorithm that run on the testing data is shown in Figure 3-6, where the median classification scheme was found to be most optimal for seizure detection.

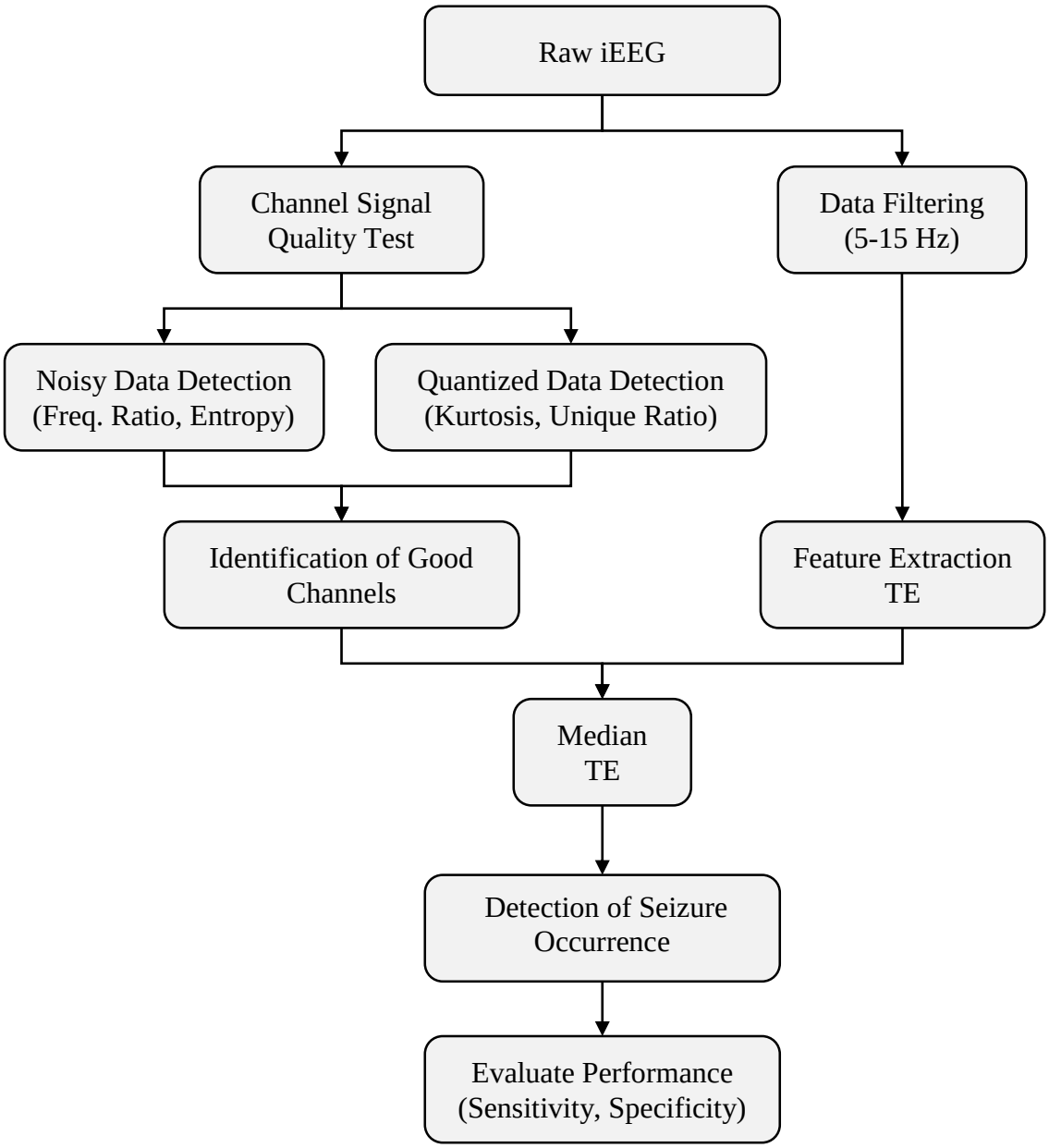

Figure 3-6: Flowchart of the optimized seizure detection scheme

This flowchart represents the final form of the algorithm; however, in the final form of the algorithm, the block for evaluating the performance is not used. The algorithm, instead, ends at the block for detection of seizures occurrence.

CHAPTER 4

RESULTS

4.1 Channel Signal Quality

The sensitivity and specificity values from the channel signal quality algorithm optimized on the training dataset are given in Table 4-1. Noisy data would negatively impact the seizure detection algorithm; however, our uncertainty on the effects that quantized data would have on the seizure detection algorithm lead us to find the optimal values for two sections of signal quality, only excluding noisy data and excluding noisy and quantized data.

Table 4-1: Performance of the section of signal quality channels from the training datasets.

	Sensitivity (%)	**Specificity (%)**
Noisy and Quantized Data Excluded	81.0	94.0
Noisy Data Excluded	81.0	95.2

As Table 4-1 shows, the algorithm was very specific (>90%) and acceptably (>80%) sensitivity to detection of noise and quantized channels following optimization of its parameters from the training datasets. The thresholds listed in Table 4-2 were selected for the channel signal quality algorithm through optimization of the training data.

Unacceptable channel signal quality had an entropy value above 0.983, a frequency ratio below 2.42, a kurtosis value greater than 743, or a unique value ratio less than 0.000105

Table 4-2: Optimized threshold values for each of the channel signal quality metrics.

Entropy	Frequency Ratio	Kurtosis	Unique Ratio
0.983	2.42	743	0.000105

The respective sensitivity and specificity values from running the channel signal quality algorithm on the testing datasets are seen in Table 4-3.

Table 4-3: Performance of the channel signal quality algorithm from the testing datasets.

	Sensitivity (%)	Specificity (%)
Noisy and Quantized Data Excluded	80.5	92.9
Noisy Data Excluded	73.2	95.3

From Table 4-3 we see that the sensitivity and specificity of the channel signal quality algorithm were 80.5% and 92.9% respectively on the testing data with the optimal thresholds identified in Table 4-2 after removing channels with noise or quantization data quality issues. The algorithm performed on testing datasets comparable to the training datasets with a sensitivity of 73.2% and a specificity of 95.3% when only the noisy channels were removed from the testing data, that is, the algorithm's sensitivity decreased by 7.3%, its specificity increased by 2.4%.

4.2 Seizure Detection

Figure 4-1 displays 2 minutes of raw iEEG data that contains a detected seizure.

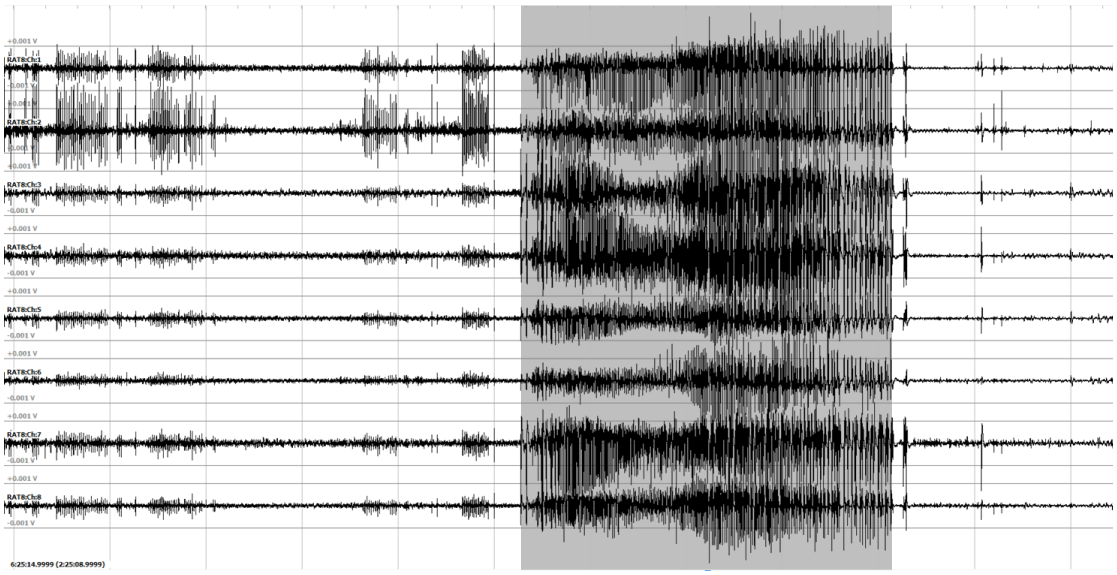

Figure 4-1: Raw iEEG data of a seizure event from the LaTech rodent study.

The channels of the iEEG are in descending order with channel 1 at the top and channel 8 at the bottom. This seizure begins at 6:26:08 AM and ends at 6:26:48 AM. Non-seizure artifacts can be seen on each side of the highlighted seizure, but these are not picked up as FPs as shown in Figure 4-2.

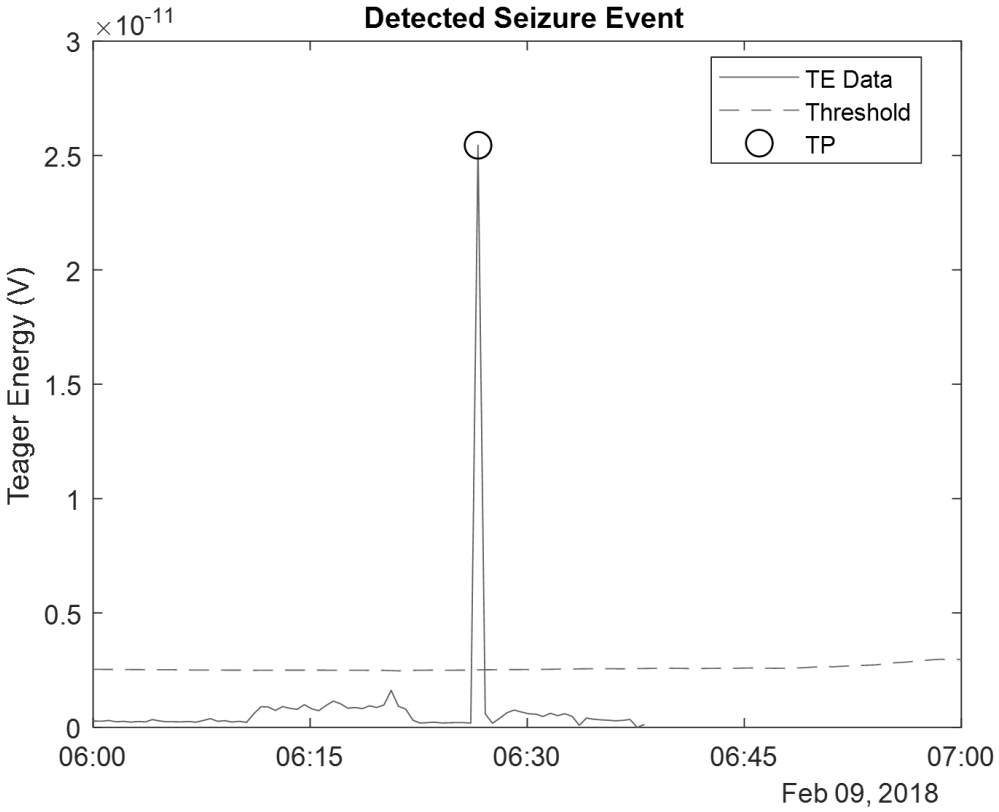

Figure 4-2: An example of a detected seizure event using the adaptive median threshold and TE.

The adaptive threshold correctly adjusted with changes in the data and the seizure event was detected. The adaptive threshold prevents FP from being detected in this data, and the median threshold used in this figure is not harshly affected by the high amplitude spike in TE due to seizure activity. The seizure event is marked with a circle at 6:26:36 AM to demonstrate that it has been detected as a TP.

The three thresholds definitions for seizure detection were assessed on the testing datasets and yielded the seizure detection results shown in Table 4-5.

Table 4-4: Threshold type results on classification of channels from the training datasets with their optimal window sizes (Wind) and scaling factors.

Channel Filtering	Thresh	Sensi (%)	FPR (FP/hr)	Wind (s)	Scaling Factor	Top Left Distance
Noisy Channels Excluded	IQR	82.5	0.127	690	8.35	17.5
	Median	87.3	0.136	240	5.23	12.7
	Median +STD	78.8	0.103	1410	4.77	21.2
Quantized and Noisy Channels Excluded	IQR	82.5	0.073	690	8.35	17.5
	Median	90.3	0.087	240	4.63	9.70
	Median +STD	82.8	0.129	1080	4.27	17.2
No Channels Excluded	IQR	83.9	0.155	690	8.26	16.1
	Median	80.0	0.185	300	8.60	20.0
	Median +STD	77.9	0.081	1440	5.02	22.1

The median threshold had the lowest top left distance of the three threshold definitions in two of the three cases of channels for the training data. The sensitivity (Sensi) for the median threshold remained quite high at >80% and nearing or exceeding 90% for two of the three cases of channels. None of the other thresholds were able to produce a sensitivity greater than 84%; however, the median threshold had a higher FPR than the other thresholds. These higher FPRs did not have as great of an impact on the top left distance since the median threshold had significantly higher sensitivities on average. The optimal parameters from the training data were applied to the testing data with the same three cases of channels in Table 4-5.

Table 4-5: Threshold type results on classification of channels from the testing datasets with their optimal window sizes (Wind) and scaling factors.

Channel Filtering	Thresh	Sensi (%)	FPR (FP/hr)	Wind (s)	Scaling Factor	Top Left Distance
Noisy Channels Excluded	IQR	63.2	0.125	690	8.35	36.8
	Median	67.7	0.600	240	5.23	32.3
	Median +STD	52.9	0.162	1410	4.77	47.1
Quantized and Noisy Channels Excluded	IQR	62.6	0.095	690	8.35	37.4
	Median	81.5	0.593	240	4.63	18.5
	Median +STD	56.8	0.268	1080	4.27	43.2
No Channels Excluded	IQR	65.2	0.156	690	8.26	34.8
	Median	59.5	0.221	300	8.60	40.5
	Median +STD	53.3	0.133	1440	5.02	46.7

The results from Table 4-5 are similar to those in Table 4-4. The median threshold has the lowest top left distance of the three threshold definitions in two of the three cases of channels. However, the sensitivities have dropped and the FPR have increased. The median threshold is the optimal threshold with a sensitivity of 81.5% and a FPR of 0.593 when both the noisy and quantized channels are excluded.

The optimization for the seizure detection algorithm was run for three cases of channels. The first case when time both the quantized and the noisy channels were removed. The second case when only the noisy channels were removed, and the last time no channels were removed. Results from all three of these rounds of optimization are summarized in Table 4-6.

The threshold that used the offset median consistently produced the highest sensitivities across all 3 cases of included channels. This threshold did not always have

the lowest FPR, but because the other thresholds exhibited much lower sensitivities, the "distance to the upper left corner of the ROC curve" was much shorter for the offset median threshold than for the other two thresholds and hence it was declared the most optimal of the three thresholds to use for seizure detection.

Table 4-6: Average performance statistics of the seizure detection algorithm across subjects from the training dataset.

	Average Sensitivity (%)	Average FPR	Window (s)	Scaling Factor
Quantized and Noisy Channels Excluded	87.3	0.136	240	5.23
Noisy Channels Excluded	90.3	0.087	240	4.63
No Channels Excluded	80.0	0.185	300	8.60

Table 4-6 lists the performance results in first case of channels inclusion with the adaptive threshold from the training data sets. In this case, the seizure detection algorithm exhibited a sensitivity of 87.3% and a FPR of 0.136 with a window size of 240 seconds and a threshold scaling factor of 5.23. In the second case of channel inclusion sensitivity of 90.3% and FPR of 0.087 from a window size of 240 seconds and a threshold scaling factor of 4.63 were observed. In the third case of channel inclusion, sensitivity of 80.0% and FPR of 8.60 per hour with a window size of 300 seconds and a threshold scaling factor of 8.60 were observed. While all sensitivities were at or above 80%, the lowest FPR for seizure detection was achieved when both noisy and quantized channels were excluded. All of FPRs were higher than the average seizure rate (SZR) of 0.021 per hour. A breakdown of the results on the training datasets for each subject can be found in the Appendix.

The average performance results over all rats of the seizure detection algorithm that was run on the testing datasets with all optimized parameters per rat are shown in Table 4-7.

Table 4-7: Average performance statistics of the seizure detection algorithm across subjects from the testing dataset

	Average Sensitivity (%)	Average FPR	Window (s)	Scaling Factor
Quantized and Noisy Channels Excluded	67.7	0.600	240	5.23
Noisy Channels Excluded	81.5	0.593	240	4.63
No Channels Excluded	59.5	0.221	300	8.60

The average sensitivities for the three cases of channel inclusion were 67.7%, 81.5%, and 59.5%, and the FPRs were 0.600, 0.593, and 0.221 per hour, respectively. The average SZR for the testing data was 0.040 seizures per hour, that is, about five times less than the lowest manifested FPRs of the seizure detection algorithm which leaves room for improvement of the algorithm. The highest sensitivity was calculated when noisy channels were excluded, and the lowest FPR was achieved when no channels were excluded.

CHAPTER 5

CONCLUSION

We built a seizure detection algorithm for seizures recorded from multi-channel long-term (years) iEEG in the lithium-pilocarpine animal model of epilepsy. The algorithm uses a two-stage process for analysis of the data. In the first stage, channels with high quality recorded iEEG are selected with a channel signal quality algorithm developed in-house where thresholds were optimized on the basis of entropy, frequency ratio, kurtosis, and unique ratio measures. In the second stages the measure of Teager-Kaiser energy was utilized to develop a metric for detection of seizure events, the algorithm was optimized on 4,981.8 hours of training datasets and then ran on 32,736.8 hours of testing datasets from 57 epileptic rats and 13 control rats. Its best ROC performance on the testing datasets across rats was 81.5% sensitively-wise with an average false positive rate of 0.593 false detections per hour or else 1 false detection per 1.69 hours that in one data is translated to false detection per seizure occurrence. Their performance is on par with the best algorithms in the literature and highlights the need for improvement of specificity of seizure detection algorithms.

Several insights were generated through this research study. The sensitivity and specificity of the channel signal quality algorithm were lower from the testing than the training datasets as expected. In every case that the signal quality algorithm excluded

channels, the FPR fell. The specificity was higher when noisy data were excluded. As it is shown in Table 4-5, the best adaptive threshold for the channel signal quality selection was the median offset. The usefulness of the channel signal quality algorithm is shown by the training and testing results of the seizure detection algorithm.

Both quantized and noisy channels should be excluded for the seizure detection algorithm to decrease its FPR. Although the sensitivity did decrease in the testing data when the signal quality algorithm excluded channels verses not excluding any channels for further analysis by the seizure detection algorithms, the decrease was not significant (from 90.3% to 81.5%). However, the decrease of the FPR was more significant when low-quality channels were excluded (from 0.087 per hour to 0.593 per hour). The decrease in sensitivity is even less significant when considering how many more hours were analyzed in the testing data (32,736.8 hours) when compared to the training data (4,981.8 hours).

If the epileptic focus is known prior to a seizure detection analysis then the analysis could be restricted to the electrodes that record the EEG from the patient's focal area. Restricting the number of electrodes would decrease the analysis time, and it would allow for greater sensitivity and specificity.

The results from this study indicate that the current algorithm has a high sensitivity even without being trained to a specific subject. The exhibited high sensitivity implies that TE is a critical feature for seizure detection.

Future improvements of the algorithm include: 1) the FPR could be lowered further by training and optimizing all parameters of the algorithm to each subject running it to detect seizures from the testing dataset of the same subject. 2) The IQR threshold

may perform better if the median TE value is calculated over overlapping 30 second windows since the IQR Rule is based on the assumption that the data follows a normal distribution, and by thus having more TE values to analyze we would increase the probability that the TE data would conform to a normal distribution. 3) The signal quality algorithm could be improved by classifying epochs of a channel as opposed to classifying the entire channel. By operating on shorter than 15 min windows, we could thus keep the most amount of acceptable data. Changing the window size would also affect the optimal values of the thresholds that could improve the performance of the channel signal quality algorithm and the subsequent performance of the seizure detection algorithm.

APPENDIX

SUPPLEMENTARY TABLES AND FIGURES

Table A-1 contains the sensitivities from the training data for the cases of the channels for each subject. Subjects without seizures are not included since sensitivity cannot be calculated in this situation.

Table A-1: Training sensitivity results for each subject.

Subjects	Sensitivity (%) Noisy Excluded	Sensitivity (%) QD & Noisy Excluded	Sensitivity (%) None Excluded
Cohort 2			
EP11	100	100	100
EP66	100	100	100
EP77	100	100	100
EP88	100	100	100
Cohort 3			
EP33	100	100	100
EP44	37.5	37.5	25.0
EP66	100	100	100
Cohort 4			
Rat1	100	100	100
Rat2	100	100	100
Rat5	100	100	100
Rat8	67.7	74.2	45.2
Cohort 5			
Rat5	33.3	66.7	33.3
Cohort 6			
Rat1	50	50	50
Rat5	100	100	100
Rat7	52.2	56.5	30.4

Table A-2 contains the FPRs and the seizure rate (SZ Rate) from the training data for the cases of the channels for each subject. For Subjects with no recorded seizures, "No SZ" will be placed in the SZ Rate column.

Table A-2: Training FPR and SZ Rate for each subject.

Subjects	FPR Noisy Excluded	FPR QD & Noisy Excluded	FPR None Excluded	SZ Rate
Cohort 1				
Rat1	0.000	0.000	0.000	No SZ
Rat2	0.073	0.396	0.000	No SZ
Rat5	0.479	0.521	2.157	No SZ
Rat7	0.021	0.021	0.042	No SZ
Rat8	0.292	0.552	0.000	No SZ
Rat4	0.010	0.021	0.010	No SZ
Rat6	0.156	0.177	0.063	No SZ
Cohort 2				
EP11	0.427	0.657	0.063	No SZ
EP33	0.115	0.146	0.000	0.010
EP44	0.229	0.386	0.010	No SZ
EP55	0.125	0.271	0.063	No SZ
EP66	0.803	0.782	0.094	No SZ
EP77	0.887	1.220	0.136	0.031
EP88	0.125	0.365	0.000	0.021
EP22	0.167	0.313	0.000	0.042
Cohort 3				
EP11	1.606	2.065	0.010	No SZ
EP33	0.038	0.051	0.019	No SZ
EP44	0.082	0.148	0.082	0.019
EP66	0.397	0.632	0.029	0.131
Sha5	0.037	0.037	0.242	0.037
Sha2	0.315	0.325	0.178	No SZ
Sha7	0.332	0.675	0.021	No SZ
Sha8	0.472	0.609	0.535	No SZ

Table A-2 Continued: Continuation of Table A-2 from Cohort 4 through Cohort 6.

Subjects	FPR Noisy Excluded	FPR QD & Noisy Excluded	FPR None Excluded	SZ Rate
Cohort 4				
Rat1	0.042	0.105	0.011	No SZ
Rat2	0.136	0.052	0.450	0.031
Rat5	0.335	0.073	0.356	0.021
Rat7	1.531	1.321	0.587	0.010
Rat8	0.482	0.597	0.000	No SZ
Rat3	0.513	1.224	0.282	0.322
Rat4	1.165	1.386	0.252	No SZ
Rat6	0.136	0.188	0.544	No SZ
Cohort 5				
Rat1	1.538	2.092	0.115	No SZ
Rat2	2.029	2.280	1.778	No SZ
Rat5	0.011	0.011	0.000	No SZ
Rat7	0.690	0.544	0.011	0.031
Rat8	0.753	0.607	0.000	No SZ
Rat4	0.303	0.481	0.052	No SZ
Rat6	0.847	1.088	0.021	No SZ
Cohort 6				
Rat1	0.179	0.483	0.000	No SZ
Rat5	0.205	0.267	0.010	0.021
Rat7	0.839	0.808	0.787	0.041
Rat8	0.914	0.977	0.353	0.240
Rat4	1.421	0.911	0.250	No SZ
RAT2a	0.072	0.114	0.021	No SZ
RAT3a	0.600	0.560	0.020	No SZ
RAT6a	1.044	0.743	0.056	No SZ
RAT3b	3.265	0.990	1.812	No SZ
RAT2b	0.053	0.032	0.000	No SZ
RAT6b	0.157	0.262	0.000	No SZ

Table A-3 contains the sensitivities from the testing data for the cases of the channels for each subject. Subjects without seizures are not included since sensitivity cannot be calculated in this situation.

Table A-3: Testing data sensitivity results for seizure detection

Subjects	Sensitivity (%) Noisy Removed	Sensitivity (%) QD & Noisy Removed	Sensitivity (%) None Removed
Cohort 2			
EP11	75.0	75.0	62.5
EP55	83.3	83.3	83.3
EP66	63.1	64.8	50.7
EP77	100	100	93.3
EP88	100	100	100
Cohort 3			
EP11	100	100	100
EP33	100	100	100
EP44	66.7	66.7	44.4
EP66	100	100	100
Cohort 4			
Rat1	66.7	66.7	66.7
Rat2	80.0	80.0	60.0
Rat8	61.6	66.5	45.2
Cohort 5			
Rat5	90.9	90.5	90.9
Rat7	100	100	100
Rat8	100	100	100
Cohort 6			
Rat1	93.8	93.8	93.8
Rat5	62.5	62.5	62.5
Rat7	66.1	67.1	51.9
Rat4	26.3	31.3	42.5

Table A-4 contains the FPRs from the testing data for the cases of the channels for each subject. For Subjects with no recorded seizures, “No SZ” will be placed in the SZ Rate column.

Table A-4: Testing data FPR and SZ Rate results for seizure detection.

Subjects	FPR Noisy Removed	FPR QD & Noisy Removed	FPR None Removed	SZ Rate
Cohort 1				
Rat1	0.007	0.034	0.000	No SZ
Rat2	0.138	0.381	0.000	No SZ
Rat5	1.744	0.099	2.222	No SZ
Rat7	0.484	0.637	0.289	No SZ
Rat8	0.138	0.242	0.000	No SZ
Rat3	0.109	0.015	1.976	No SZ
Rat4	0.009	0.040	0.068	No SZ
Rat6	0.110	0.173	0.062	No SZ
Cohort 2				
EP11	1.548	2.062	0.237	0.003
EP33	0.015	0.030	0.007	0
EP44	0.432	0.698	0.074	0
EP55	0.185	0.300	0.086	0.014
EP66	0.717	0.939	0.193	0.074
EP77	1.064	1.342	0.356	0.007
EP88	0.410	0.752	0.012	0.025
EP22	0.302	0.526	0.007	0
Cohort 3				
EP11	0.861	1.096	0.044	0.010
EP33	0.042	0.050	0.010	0.013
EP44	0.355	0.503	0.248	0.076
EP66	0.531	0.726	0.094	0.008
Sha5	0.102	0.014	0.175	No SZ
Sha2	0.385	0.581	0.128	No SZ
Sha7	0.175	0.289	0.004	No SZ
Sha8	0.307	0.550	0.310	No SZ

Table A-4 Continued: Continuation of Table A-4 from Cohort 4 through Cohort 6.

Subjects	FPR Noisy Removed	FPR QD & Noisy Removed	FPR None Removed	SZ Rate
Cohort 4				
Rat1	0.776	0.987	0.369	0.032
Rat2	0.311	0.248	0.331	0.016
Rat5	0.088	0.211	0.059	0
Rat7	1.858	0.671	1.703	No SZ
Rat8	0.333	0.502	0.062	0.109
Rat3	0.496	0.864	0.025	No SZ
Rat4	1.230	1.477	0.184	No SZ
Rat6	0.500	0.337	0.449	No SZ
Cohort 5				
Rat1	0.694	0.953	0.056	No SZ
Rat2	0.751	0.779	0.550	No SZ
Rat5	0.024	0.029	0.011	0.051
Rat7	0.554	0.425	0.006	No SZ
Rat8	0.703	0.703	0.033	0.254
Rat3	1.584	1.556	0.074	No SZ
Rat4	0.168	0.220	0.073	0
Rat6	0.751	0.880	0.034	0
Cohort 6				
Rat1	0.473	0.798	0.009	0.065
Rat5	0.630	0.725	0.046	0.017
Rat7	0.916	0.816	0.626	0.329
Rat8	0.847	1.217	0.168	No SZ
Rat4	1.069	0.776	0.132	0.206
RAT2a	0.005	0.012	0.007	No SZ
RAT3a	0.588	0.622	0.016	No SZ
RAT6a	1.070	0.860	0.120	0
RAT3b	3.120	1.050	1.185	No SZ
RAT2b	0.031	0.069	0.003	No SZ
RAT6b	0.476	0.780	0.003	No SZ
RAT3c	0.321	0.187	1.456	No SZ

BIBLIOGRAPHY

[1] I. Rektor *et al.*, “Epilepsy, behavior, and art (Epilepsy, Brain, and Mind, part 1),” *Epilepsy Behav.*, vol. 28, no. 2, pp. 261–282, 2013.

[2] World Health Organization, “Epilepsy Fact Sheet,” *World Health Organization*, 2018. [Online]. Available: http://www.who.int/mediacentre/factsheets/fs999/en/. [Accessed: 05-Mar-2018].

[3] M. M. Zack and R. Kobau, “National and State Estimates of the Numbers of Adults and Children with Active Epilepsy — United States, 2015,” *Morb. Mortal. Wkly. Rep.*, vol. 66, no. 31, pp. 821–825, Aug. 2017.

[4] World Health Organization, *Atlas: Epilepsy Care in the World*. Geneva: World Health Organization, 2005.

[5] Mayo Clinic, “Epilepsy,” *Mayo Clinic*, 2018. [Online]. Available: https://www.mayoclinic.org/diseases-conditions/epilepsy/symptoms-causes/syc-20350093. [Accessed: 05-Mar-2018].

[6] Medline Plus, “Epilepsy,” *Medline Plus*, 2017. [Online]. Available: https://medlineplus.gov/epilepsy.html. [Accessed: 05-Mar-2018].

[7] National Institute of Neurological Disorders and Stroke, “Epilepsy Information Page,” *National Institute of Neurological Disorders and Stroke*, 2017. [Online]. Available: https://www.ninds.nih.gov/Disorders/All-Disorders/Epilepsy-Information-Page. [Accessed: 05-Mar-2018].

[8] Centers for Disease Control and Prevention, “Epilepsy,” *Centers for Disease Control and Prevention*, 2018. [Online]. Available: https://www.cdc.gov/epilepsy/about/types-of-seizures.htm. [Accessed: 05-Mar-2018].

[9] T. Tomson, R. Surges, R. Delamont, S. Haywood, and D. C. Hesdorffer, “Who to target in sudden unexpected death in epilepsy prevention and how? Risk factors, biomarkers, and intervention study designs,” *Epilepsia*, vol. 57, pp. 4–16, 2016.

[10] O. Devinsky, D. C. Hesdorff, D. J. Thurman, S. Lhatoo, and G. Richerson, “Sudden unexpected death in epilepsy : epidemiology , mechanisms , and prevention,” *Lancet Neurol.*, vol. 15, no. 10, pp. 1075–1088, 2016.

[11] C. Harden *et al.*, “Practice guideline summary: Sudden unexpected death in

epilepsy incidence rates and risk factors," *Neurology*, vol. 88, no. 17, pp. 1674–1680, Apr. 2017.

[12] S. Agrawal, L. Turco, S. Goswami, M. Faulkner, and S. Singh, "Yield of Monitoring in an Adult Epilepsy Monitoring Unit (P2.097)," *Neurology*, vol. 84, no. 14 Supplement, Apr. 2015.

[13] B. D. Moseley, S. Dewar, Z. Haneef, D. Eliashiv, and J. M. Stern, "Reasons for prolonged length of stay in the epilepsy monitoring unit," *Epilepsy Res.*, vol. 127, pp. 175–178, Nov. 2016.

[14] S. R. Sinha *et al.*, "American Clinical Neurophysiology Society Guideline 1: Minimum Technical Requirements for Performing Clinical Electroencephalography," *J. Clin. Neurophysiol.*, vol. 33, no. 4, pp. 303–307, 2016.

[15] Y. Wang, X. Long, H. Van Dijk, R. Aarts, and J. Arends, "Adaptive EEG Channel Selection for Nonconvulsive Seizure Analysis," in *2018 IEEE 23rd International Conference on Digital Signal Processing (DSP)*, 2018, pp. 1–5.

[16] L. J. Gabard-Durnam, A. S. Mendez Leal, C. L. Wilkinson, and A. R. Levin, "The Harvard Automated Processing Pipeline for Electroencephalography (HAPPE): Standardized Processing Software for Developmental and High-Artifact Data," *Front. Neurosci.*, vol. 12, no. February, pp. 1–24, 2018.

[17] S. Rheims *et al.*, "Automatic bad channel detection in intracranial electroencephalographic recordings using ensemble machine learning," *Clin. Neurophysiol.*, vol. 129, no. 3, pp. 548–554, 2017.

[18] K. A. Robbins, K.-M. Su, T. Mullen, C. Kothe, and N. Bigdely-Shamlo, "The PREP pipeline: standardized preprocessing for large-scale EEG analysis," *Front. Neuroinform.*, vol. 9, no. June, pp. 1–20, 2015.

[19] E. Nordqvist, M. Rudner, M. Johansson, M. Lindgren, and M. Heimann, "The relationship between deferred imitation, associative memory, and communication in 14-months-old children. Behavioral and electrophysiological indices," *Front. Psychol.*, vol. 6, no. MAR, pp. 1–12, 2015.

[20] R. D. Thomas, N. C. Moses, E. A. Semple, and A. J. Strang, "An efficient algorithm for the computation of average mutual information: Validation and implementation in Matlab," *J. Math. Psychol.*, vol. 61, pp. 45–59, Aug. 2014.

[21] A. Ulate-Campos *et al.*, "Automated seizure detection systems and their effectiveness for each type of seizure," *Seizure*, vol. 40, pp. 88–101, 2016.

[22] N. Ozdemir and E. Yildirim, "Patient Specific Seizure Prediction System Using Hilbert Spectrum and Bayesian Networks Classifiers," *Comput. Math. Methods Med.*, vol. 2014, pp. 1–10, 2014.

[23] K. Gadhoumi, J. Gotman, and J. M. Lina, “Scale Invariance Properties of Intracerebral EEG Improve Seizure Prediction in Mesial Temporal Lobe Epilepsy,” *PLoS One*, vol. 10, no. 4, p. e0121182, Apr. 2015.

[24] Y. Park, L. Luo, K. K. Parhi, and T. Netoff, “Seizure prediction with spectral power of EEG using cost-sensitive support vector machines,” *Epilepsia*, vol. 52, no. 10, pp. 1761–1770, Oct. 2011.

[25] S. F. Liang, H. C. Wang, and W. L. Chang, “Combination of EEG complexity and spectral analysis for epilepsy diagnosis and seizure detection,” *EURASIP J. Adv. Signal Process.*, vol. 2010, pp. 17–20, 2010.

[26] R. A. Lewis, B. Parks, and A. M. White, “Determination of Epileptic Seizure Onset from EEG Data Using Spectral Analysis and Discrete Finite Automata,” *Nan*, vol. nan, no. nan.

[27] D. M. Treiman, “GABAergic mechanisms in epilepsy.,” *Epilepsia*, vol. 42 Suppl 3, pp. 8–12, 2001.

[28] V. R. Solomon, V. J. Tallapragada, M. Chebib, G. A. R. Johnston, and J. R. Hanrahan, “GABA allosteric modulators: An overview of recent developments in non-benzodiazepine modulators,” *Eur. J. Med. Chem.*, vol. 171, pp. 434–461, Jun. 2019.

[29] Tucker-Davis Technologies, *RPvdsEx Manual*. Alachua, Florida, USA: Tucker-Davis Technologies, 2016.

[30] A. O. Boudraa and F. Salzenstein, “Teager–Kaiser energy methods for signal and image analysis: A review,” *Digit. Signal Process. A Rev. J.*, vol. 78, no. March, pp. 338–375, 2018.

[31] E. Kvedalen, “Signal processing using the Teager Energy Operator and other nonlinear operators,” University of Oslo, 2003.

[32] F. Ulaby and A. Yagle, *Engineering Signals and Systems*, 1st ed. National Technology & Science Press, 2012.